The effect of liquid nitriding on the corrosion resistance of AISI 304 austenitic stainless steel in H2S environments

Li, Longyi; Wang, Jun ; Yan, Jing; Duan, Liang; Li, Xiaoying; Dong, Hanshan

DOI:
10.1007/s11661-018-4920-9

The effect of liquid nitriding on the corrosion resistance of AISI 304 austenitic stainless steel in H_2S environments

Longyi Li [a], Jun Wang [a*], Jing Yan [b], Lian Duan [a], Xiaoying Li [c], Hanshan Dong [c]

a College of Manufacturing Science and Engineering, Sichuan University, 610065, Chengdu, PR China

b Research Institute of Natural Gas Technology, PetroChina Southwest Oil and Gas Field Company, 610213, Chengdu, PR China.

c School of Metallurgy and Materials, University of Birmingham, Edgbaston, Birmingham B15 2TT, UK

Abstract: AISI 304 austenitic stainless steel was low-temperature liquid nitrided in a molten salt bath at 703 K for 8 h, which produced a 3-layered structure consisting of a top oxide layer, an intermediate nitrogen-rich layer and a bottom carbon-rich layer. The effect of nitriding on its corrosion resistance was investigated in a H_2S environment. The corrosion rate of the untreated sample is about 3.3 times that of the nitrided sample after H_2S corrosion. Corrosion pits can be clearly observed on the surface of the untreated sample, while the nitrided sample surface remained relatively intact. Both the oxide layer and the nitrogen-rich layer can help reduce the hydrogen permeation, which is beneficial for combating hydrogen embrittlement. The corrosion products mainly consisted of oxides, hydroxides, and sulfates. The nitrided layers can serve as a barrier to corrosion, thus preventing the corrosion of the substrate material. Active nitrogen in the nitrided layer reacts with H ions to form NH_4^+, which effectively prevents further acidification of the local area and inhibits the occurrence of pitting corrosion and the dissolution rate of the metal in the etching hole, thus improving the local corrosion resistance of the stainless steel.

Key words: austenite stainless steels, expand austenite, corrosion resistance, liquid nitriding, surface treatment

1. Introduction

Austenite stainless steel is widely used in various industrial fields due to its excellent corrosion resistance and mechanical properties. With the increasing exploitation and processing of high sulfur oil and gas field, H_2S corrosion has become a widespread concern.[1] H_2S is one of the most dangerous factors causing metal corrosion in acidic oil and gas environments, and electrochemical corrosion will occur on the surface of the pipeline used.[2] In recent years, many researchers have conducted extensive research on the local corrosion and stress corrosion cracking (SCC) mechanism of stainless steel in H_2S medium. The research was focused on the

* Corresponding author. E-mail address: Srwangjun@scu.edu.cn (J. Wang)

structure, properties, formation process and external factors of corrosion products in saturated H_2S systems.[3-6] Ding et al. investigated the behavior of corrosion and SCC of austenitic stainless steels in high H_2S–CO_2–Cl^- environments. [7] Their results showed that high H_2S–CO_2 pressure can accelerate anodic dissolution process, deteriorate passive films, and aggravate SCC sensitivity. The corrosion rate of steel in wet H_2S is significantly higher than that in dry H_2S environment.[8] H_2S reacted with metals to form surface metal sulfides, and released hydrogen atoms, which were absorbed by the metal surface and caused hydrogen embrittlement.[9] Besides, low pH can promote both cathodic and anodic actions on stainless steel and facilitate passive film breakdown.[7]

In addition to the corrosion of H_2S, CO_2 and Cl^-, saturated natural gas in pipelines will have a free liquid phase due to the effect of pressure drop, and a certain amount of solid impurities will be mixed in the pipeline, resulting in three-phase coexistence of gas, solid, and liquid. Erosion-corrosion is faster than corrosion alone and is a more hazardous local corrosion.[10] When corrosive liquid contains solid particles (such as insoluble salts, sand, drilling fluid, etc.), it is more likely to cause such erosion-corrosion damage. Austenitic stainless steels have a low carbon content (mass fraction below 0.03 %), resulting in a low surface hardness and poor wear resistance. The service life of stainless steel pipes under such conditions will be seriously reduced， and so it is necessary to improve their surface hardness and strength on the premise of ensuring its good comprehensive performance.

It has been reported previously that austenitic stainless steels are thermochemically treated (carburized or nitrided) at low temperatures to form interstitial atoms supersaturated non-deposition layers. [11-12] After the treatment, a layer with a high concentration of nitrogen and/or carbon will be formed on the surface of the treated austenitic stainless steel. This surface layer can effectively improve the hardness, wear resistance, fatigue resistance and corrosion resistance of the material, which is so-called S-phase or expanded austenite.[12] Low-temperature nitriding has been shown to significantly improve pitting potential. Dong discovered that low temperature nitrided 316 stainless steel showed excellent resistance to pitting of chlorine containing solution, and the increased corrosion resistance of the nitride S phase layer is thought to be due to its high nitrogen content.[13] The enhancement in corrosion resistance of austenitic stainless steels by nitriding or carbonization treatment may be related to a high surface interstitial atom concentration or a large surface residual compressive stress due to interstitial atoms.[14]

Zhang et al. performed Quench-Polish-Quench (QPQ) salt bath compound treatment on GX-8 alloy steel and found that the dense oxide film Fe_3O_4 could significantly reduce the friction coefficient of the material at 573 K, and the corrosion resistance of the material was greatly improved before the oxide film was ruptured.[15] However, the QPQ treatment is a multi-step and hence relatively complicated process. In contrast, low-temperature salt bath nitriding does not require an additional oxidation process to form a surface oxide layer. Hence, the salt bath nitriding process is simpler and the cost of the equipment is lower than the QPQ process.

The aim of the present paper was to study the effect of low-temperature liquid

bath nitriding on the corrosion resistance of AISI 304 austenitic stainless steel in a H_2S containing environment. Through the H_2S immersion corrosion tests, the corrosion behavior and the corrosion mechanism of low temperature salt bath nitride 304 austenitic stainless steel in H_2S containing environments (such as pipelines for oil and gas applications) were studied. The low-temperature nitriding is expected to be applied to the pipelines used for oil-gas fields, significantly extending their service life in the H_2S corrosion environment.

2. Experimental

2.1 Material

The material used in this experiment was cast 304 stainless steel, taken from the natural gas valve castings supplied by Southwest Natural Gas Research Institute，China. The chemical composition provided by the materials supplier is shown in Table 1. The samples were ground with abrasive papers from 400# down to 1200#, degreased with a mixture of 50 vol% ethanol and 50 vol% acetone, and finally washed with deionized water and dried in atmosphere.

Table 1 Chemical composition of AISI 304 stainless steel (mass%)

Element	C	Cr	Ni	Mn	Si	S	P	Fe
Pct	0.035	18.640	8.010	1.100	0.436	0.020	0.013	Balance

2.2 Liquid bath nitriding and H_2S corrosion test

The chemicals used in this experiment for liquid bath nitriding were non-toxic cyanate, chloride and carbonate salts. The nitriding process involved immersing the sample in 703 K molten salt for 8 hours, during which the non-toxic cyanate decomposes into carbon atoms and nitrogen atoms, forming a high chemical potential on the surface of the samples. More details can be found in literature.[16] This high chemical potential promotes the diffusion of the nitrogen and carbon atoms into the austenitic stainless steel sample, thus forming a large supersaturation of N(C) in its surface.

H_2S corrosion tests were conducted in accordance with NACE TM0177-2005 standard using the solution ‘A’ recommended by NACE TM0177-2005. Both the untreated and nitrided samples were soaked in this solution for 720 hours.

Before the H_2S corrosion test, the mass of the sample (m) was weighed and recorded. At the end of the test, the corroded sample was taken out, and the corrosion product formed on the surface was removed with an acid stripping solution (500 ml HCl + 500 ml H_2O + 3.5 g $C_6H_{12}N_4$). The sample was degreased with acetone and then dried in a box. After drying for 24 hours, the sample was taken out for weighing (m_t), and the corrosion rate was calculated based on the weight loss during the test. The uniform corrosion rate (R_{corr}) is calculated as follows: $R_{corr}=8.76\times10^4\times(m-m_t)/(S_1\times\rho\times t)$, where S_1 is the total area of the test piece (32 cm^2); ρ is the density of the test piece material (7.9 g/cm^3); and t is the test time (720 h).

2.3 Hydrogen permeation test

Hydrogen permeation testing was performed in line with ASTM G148 standard using a type Avanathan-Stachursky double-electrolytic cell produced by Wuhan Corrtest, China.[17] Three sets of samples were prepared: untreated samples, as-nitrided samples and the nitride samples whose surface oxide film was removed by mechanical polishing. The samples used in this test were stainless steel wafer electrodes with a working surface of 1.77 cm^2 and a thickness of 0.2 mm. The experimental conditions were decided by referring to literature.[18-19] The experimental solution is 0.5 mol/L sulfuric acid with 1 g/L CH_4N_2S, and the hydrogen charge current is 20 mA/cm^2 with an anode potential of 300 mV. Before the test solution was added, the sample was passivated in a 0.2 mol/L NaOH solution for more than 24 h, in order that the background current density is less than 0.1 $\mu A/cm^2$.[20]

The hydrogen diffusion flux ($J\infty$) is calculated from the anode steady-state current (I_∞) and can be expressed as:

$J\infty =$ [21]

Where: A is the area of the sample in contact with the solution; F is the Faraday constant.

The effective hydrogen diffusion coefficient (D_{eff})can be calculated using the formula below:

$D_{eff} =$ [22]

Where: t is the thickness of the sample; t_L is the delay time. The delay time is approximately equal to the time taken for the hydrogen charging current density to reach 0.63 times the steady-state anode current density, i.e. the time used for $I_a=0.63I\infty$. The hydrogen concentration C_o at the hydrogen end can be estimated by the following formula:

$C_o =$ [22]

2.4 Microstructural characterization

The cross section of the sample before and after the H_2S corrosion tests was mechanically polished and chemically etched with an etchant formulated with 50 vol% HCl, 25 vol% HNO_3, and 25 vol% H_2O. The OLYMPUS GX51 optical microscope and JSM-7500F scanning electron microscope were used for microstructural analysis. The surface phases were studied using the EMPYREAN X-ray diffractometer (XRD) with a scanning range of 20 to 110 degrees with Cu Kα radiation (λ =0.15418nm). The SHIMADZU-1720 electron probe microanalyzer (EPMA) was used to quantitatively analyze the elemental distribution from the surface to the matrix. X-ray photoelectron spectroscopy (XPS) was used to analyze the surface corrosion products.

3. Results

3.1 Characteristics of the nitrided layers

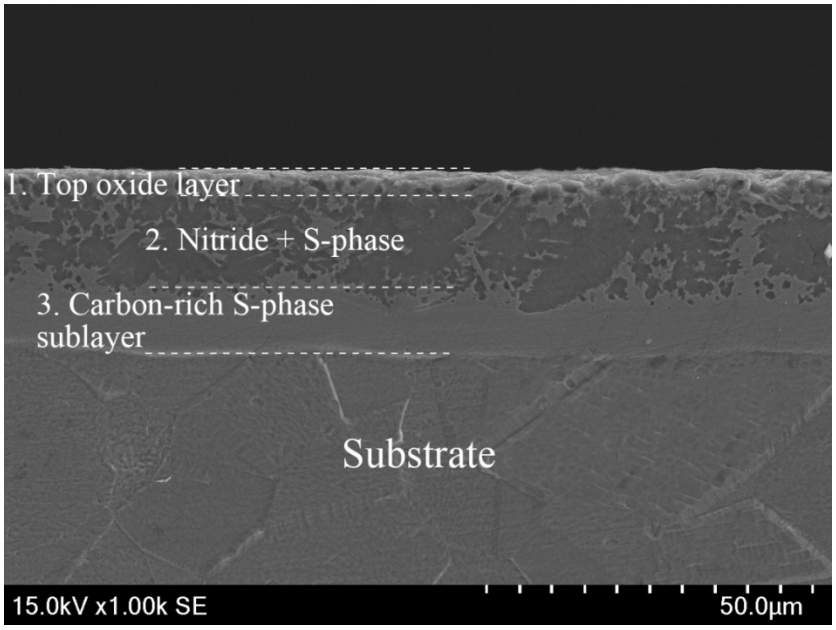

Fig.1 A typical cross sectional SEM image of nitrided sample

Figure 1 shows the cross-sectional photomicrograph of the AISI304 austenitic stainless steel after low-temperature salt bath nitriding treatment. The substrate shows clear grain boundaries after etching with the etchant. The salt bath nitriding produced a 3-layered structure consisting of an oxide top layer, followed by a nitrogen-rich layer and a carbon-rich layer. The atomic nitrogen was formed from the following CNO^- dissociation reaction: $4CNO^- \rightarrow 2CN^- + CO_3^{2-} + CO + [N]$. Carburizing is also promoted by the liberation of atomic carbon species according to the following CO dissociation reaction: $CO \rightarrow CO_2 + [C]$. Under the same treatment conditions, the thickness of the nitrided layer is larger than that of the carburized layer. This is mainly due to the fact that the atomic radius of N is smaller than that of the C atom, and the energy required for N atoms to enter the lattice is smaller than that for C atoms. Under the same conditions, the nitrogen atoms can diffuse deeper that carbon atoms. Tsujikawa et al. used simultaneous carburizing and nitriding process to obtain a similar layer on the surface of austenitic stainless steel.[23] Due to the long processing time, certain Cr nitrides appear in the nitrided layer.

3.2 Corrosion morphology and corrosion rate

Nitrided samples and as-received 304 samples were immersed in H_2S solution for 720 h and the cross-sectional micrographs are shown in the Figure 2.

As shown in Figure 2(a), a number of pits and cracks were observed from the cross-section of the untreated sample, which indicates pitting and cracking of the sample. In the process of crack propagation, the width and depth of the crack continuously increased, and the outer layer material eventually spalled off. In contrast, neither pits nor cracks were observed from the cross-section of the nitrided samples after H_2S corrosion test (Fig.2(b)).

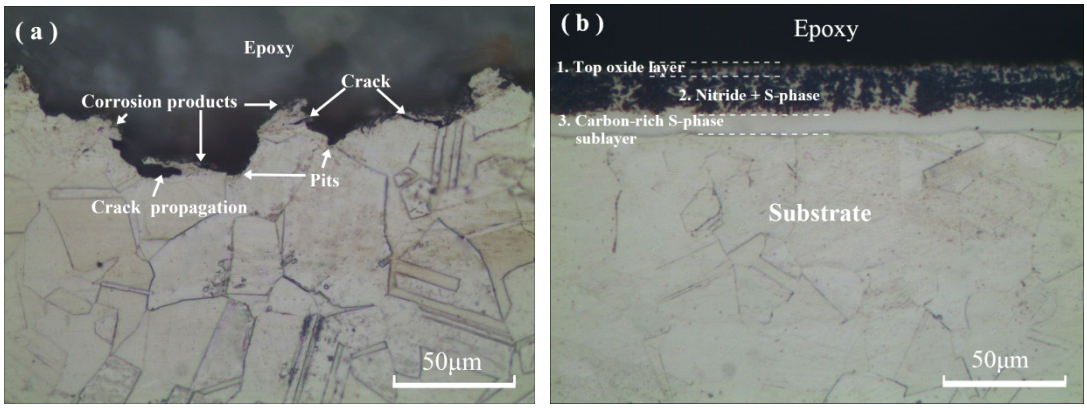

Fig.2 Cross-sectional optical micrographs (OM): (a) untreated sample (b) nitrided sample after immersion in H_2S solution for 720h

Figure 3 shows the surface morphology of the untreated and nitrided samples after immersion in H_2S solution for 720h. Many agglomerates were formed on the surface of the untreated sample (Fig.3(a)), which is generally considered to be corrosion product FeS. The surface of the nitrided sample remained intact as evidenced by the existence of the original grinding marks with almost no corrosion product (Fig.3(b)).

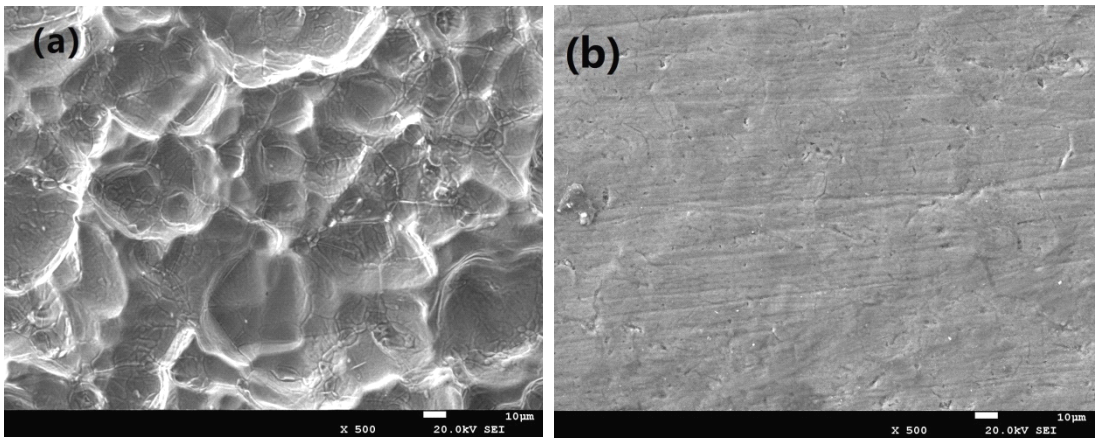

Fig.3 SEM surface corrosion morphology: (a) untreated sample (b) nitrided sample after immersion in H_2S solution for 720h

As shown in Figure 4, the corrosion rate of the untreated 304 austenitic stainless steel (0.20 mm/a) is approximately 3.3 times that of the nitrided samples (0.06 mm/a). This indicates that the nitriding treatment can significantly improve the corrosion resistance of 304 stainless steel in the H_2S environment.

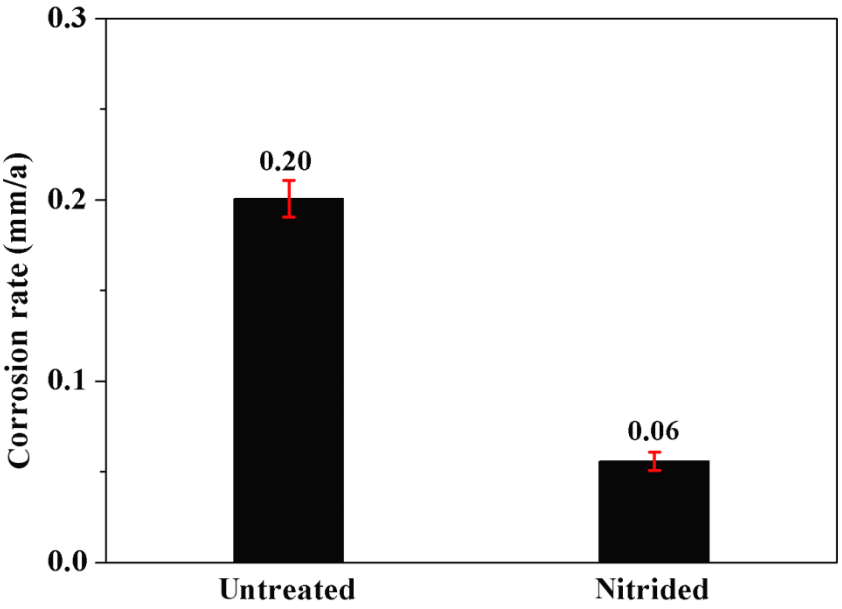

Fig.4 Corrosion rate after H_2S corrosion for 720h

The ionization of H_2S in the solution produced a large amount of H^+, which led to a significant decrease in the pH of the solution. The ionization reaction can be described as follows: $H_2S = H^+ + HS^-$; $2HS^- = 2H^+ + S^{2-}$. The ionized H^+ is a strong depolarizer that can easily take away electrons from the metal and promote the dissolution reaction of the anode steel to cause metal corrosion. The process of electrochemically etching the cathode and the anode by H_2S is as follows:

Cathode: $Fe - 2\ e^- \rightarrow Fe^{2+}$;

Anode: $2H^+ + 2e^- \rightarrow 2H \rightarrow H_2 \uparrow$.

The anode corrosion product is: $Fe^{2+} + S^{2-} = FeS\downarrow$. Therefore, after the steel is corroded by H_2S, the final product of the anode is FeS. The product usually has a defective structure with poor adhesion to the surface of steel. Hence, it can be easily detached and oxidized, and has a more positive potential. The corrosion product then acts as a cathode and the matrix to form an active microbattery and continues the corrosion of the steel. The process repeated itself and the layer eventually cracked.

3.3 XRD analysis

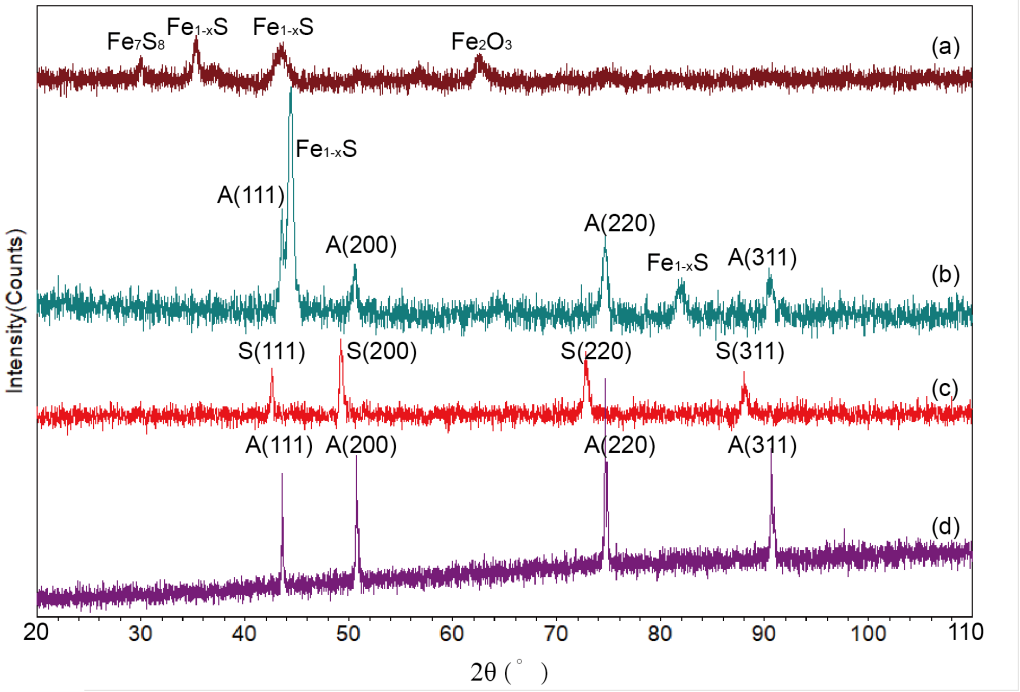

Fig.5 XRD patterns for different samples: (a) nitrided sample after corrosion test, (b) untreated sample after corrosion test, (c) as-nitrided sample and (d) untreated sample before corrosion test

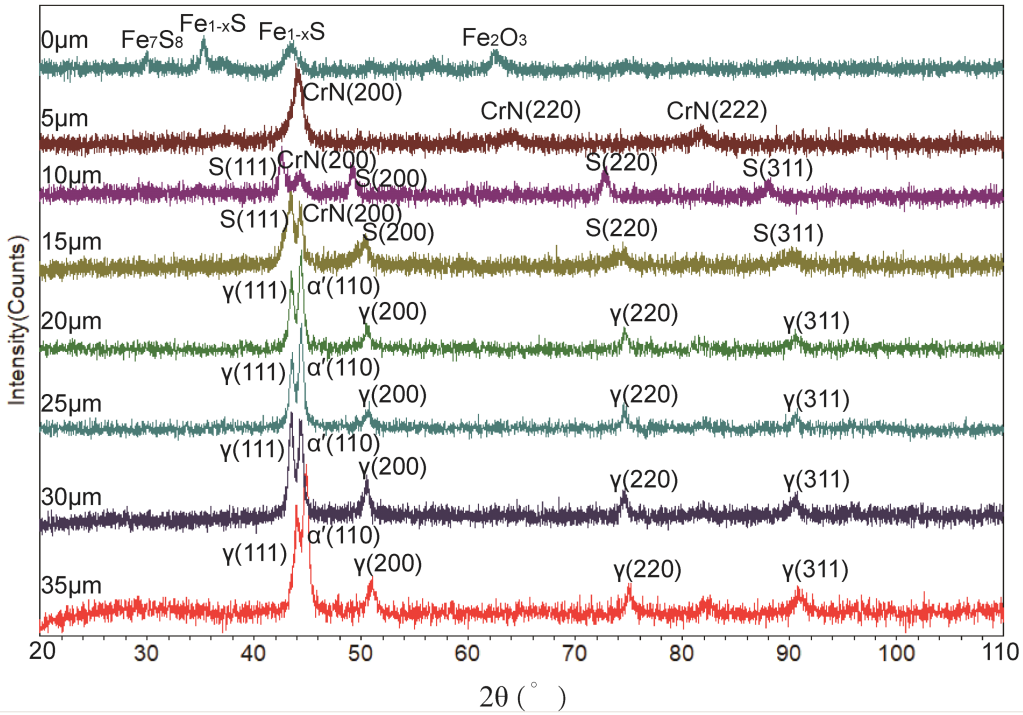

Fig. 6 XRD patterns as a function of the depth below the original nitrided surface (after mechanical material removal).

Untreated and nitrided samples were characterized by XRD to identify the phases produced as a consequence of H_2S corrosion process; the diffraction patterns of the samples are shown in Figure 5. It can be seen from Figure 5 that the untreated sample shows typical peaks for austenite (Fig.5(d)); the nitrided sample clearly shows S1(111)、S2(200)、S3(220) and S4(311) peaks. This indicates that the S-phase layer has been successfully produced during nitriding. The N or C atoms dissolved in austenite caused the expansion of the original face-centered cubic lattice of austenite (i.e. expanded austenite) and the left-shift of these peaks.[24] As shown in Figure 5(b), the corrosion product formed on the untreated sample is $Fe_{1-X}S$, which shows two peaks, one near γ(111) and the other between γ(200) and γ(311). Clear austenite characteristic peaks can still be observed on the XRD diffraction pattern of the untreated sample after H_2S corrosion. The corrosion products of the nitrided samples were mainly Fe_7S_8, $Fe_{1-X}S$, and Fe_2O_3. Compared with the untreated samples, the characteristic peaks of the expanded austenite could not be observed. This implies that the nitrogen concentrations in the ≈5 μm thick layer below the specimen surface that is sampled by the X-rays would be reduced during the H_2S corrosion test.

The XRD patterns obtained at different depths below the original surfaces are shown in Figure 6. In the depth of 5 μm, the nitrided sample exhibits three main diffraction peaks of CrN, which was formed as a consequence of the temperature of the treatment, the chromium-rich alloy AISI 304, and the high nitrogen content. When the nitrogen content gradually decreased with the depth, the intensity and the number of CrN peaks reduced accordingly. Normally, when the AISI 304 stainless steel is nitride at 703 K or below, the nitrided layer should be free of nitrides. However, the as-cast 304 stainless steel used in this research may not be well annealed after cold rolling, and a large amount of deformed martensite (α′) was left in the matrix, as evidenced by the clear α′ peak detected from the substrate (Fig. 6). This resulted in rapid nitrogen diffusion and precipitation of CrN. At the depth of 10 and 15 μm, distinct peaks of S phase and a weak CrN peak can be detected. Then, the α′-martensite phase was detected from the depth 20 μm down to the substrate, which is also contributed by the strain-induced martensite formed during the layer-by-layer mechanical polishing process. Starting from the depth of 20μm, as the interstitial atom concentration gradually decreased, the lattice distortion also gradually decreased, and it is better to call it γ-phase instead of S-phase. The content of interstitial atoms (C or N) continuously decreased with the depth and the diffraction angle of the γ-phase gradually returned to normal values.

3.4 EPMA analysis

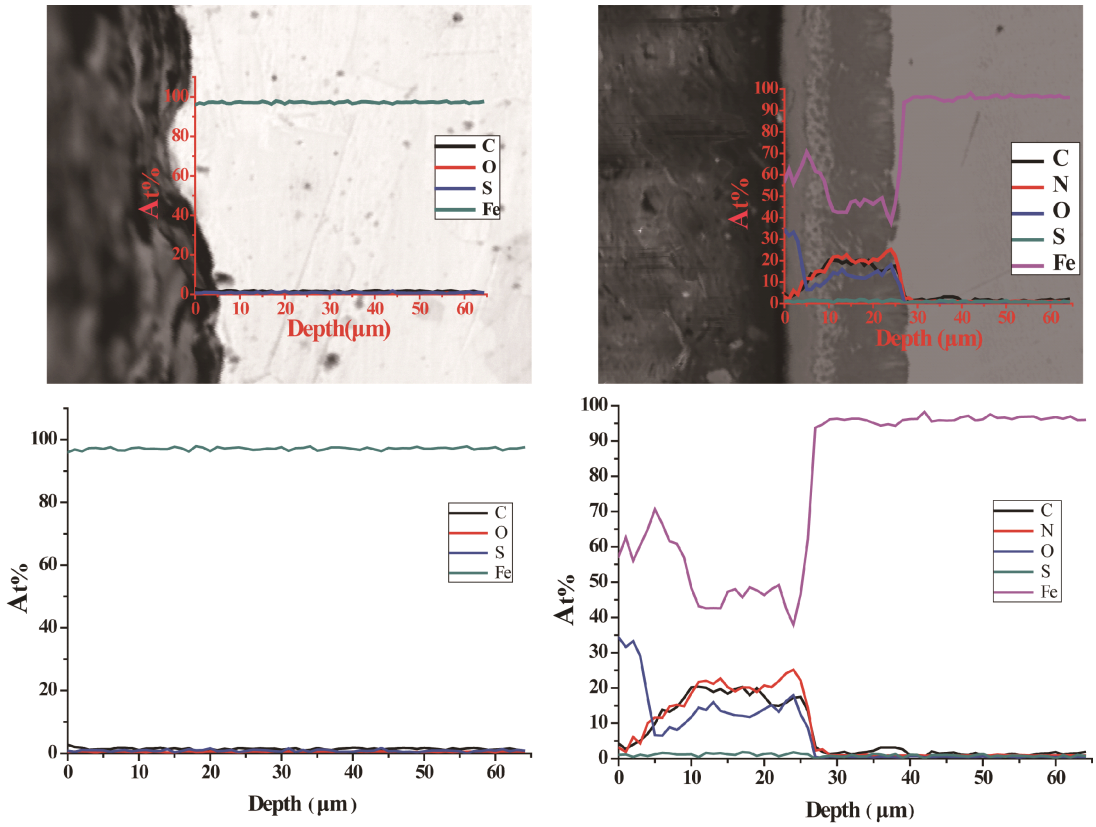

(a) (b)

Fig.7 EPMA results of untreated (a) and nitrided samples (b) after immersion corrosion test in Solution A for 720h

Figure 7 shows the EPMA results of the untreated and low temperature nitrided samples after immersion corrosion test. It can be seen by comparing Figure 7(b) with (a) that oxygen concentration increased significantly in the nitrided layer due to the oxygen atoms introduced during the nitriding process. It can be also seen that there is an oxygen plateau near the surface, which is overlapped with the grey surface layer showed in the top graph of Figure 7(b). This indicates the formation of an oxide layer during the salt bath nitriding process. The concentration of nitrogen was increased due to the formation of supersaturated austenite, which improves corrosion resistance. However, the nitrogen content decreased slightly near the surface, which may be caused by the consumption of nitrogen atoms. Combined with the results of XPS analysis, it is known that this is due to the reaction of reactive nitrogen in the nitride layer with H^+ in the H_2S solution to form NH_4^+. For the untreated sample, the iron concentration sharply declined on the surface, which means the destruction of the passivation film， thus jeopardizing the corrosion resistance of the untreated sample leading to the appearance of a large number of corrosion pits on the surface (Fig.2(a)).

3.5 XPS analysis

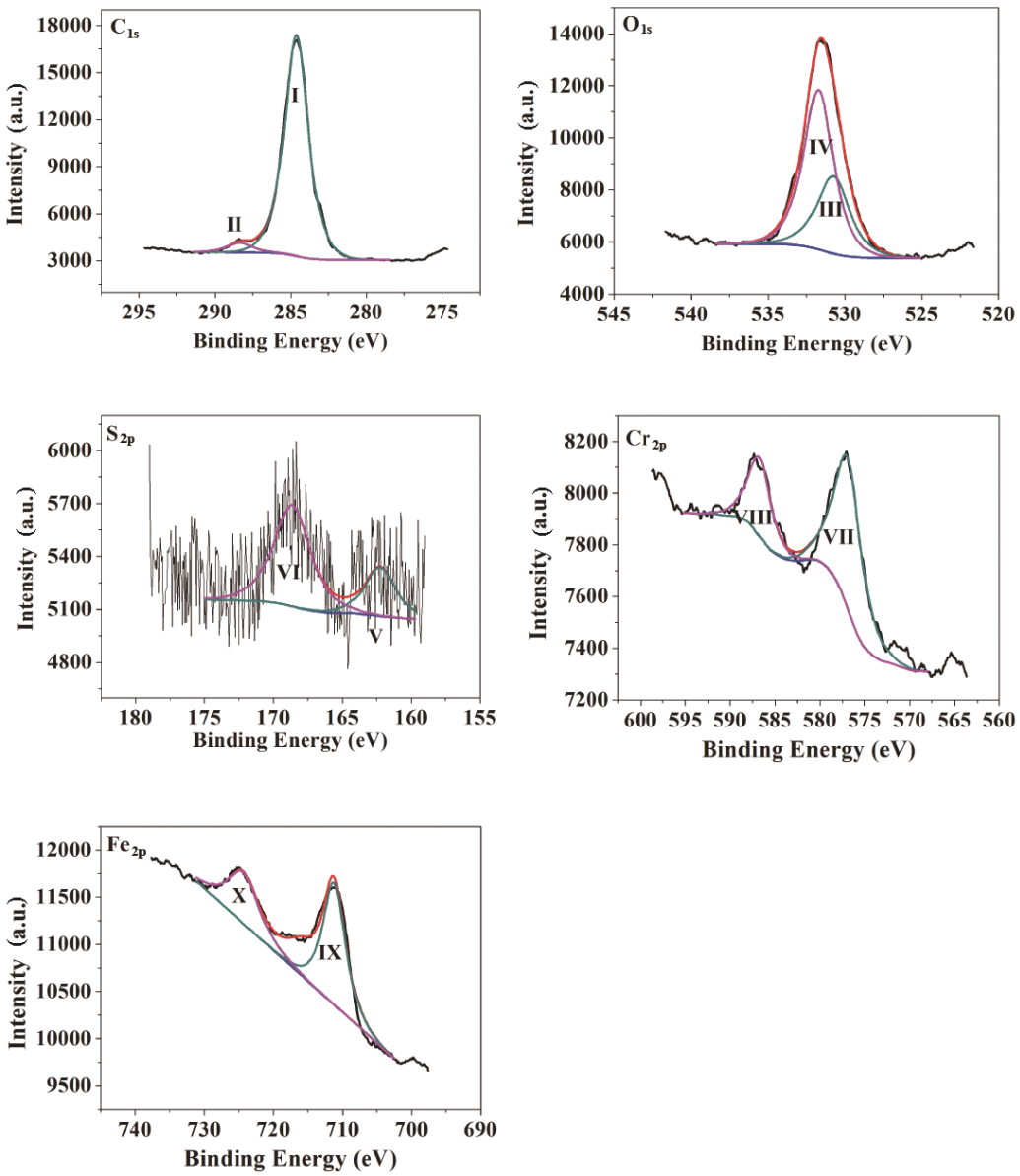

Fig.8 High resolution XPS spectra of untreated samples after H_2S corrosion: C_{1s}, O_{1s}, S_{2p}, Cr_{2p}, Fe_{2p}.

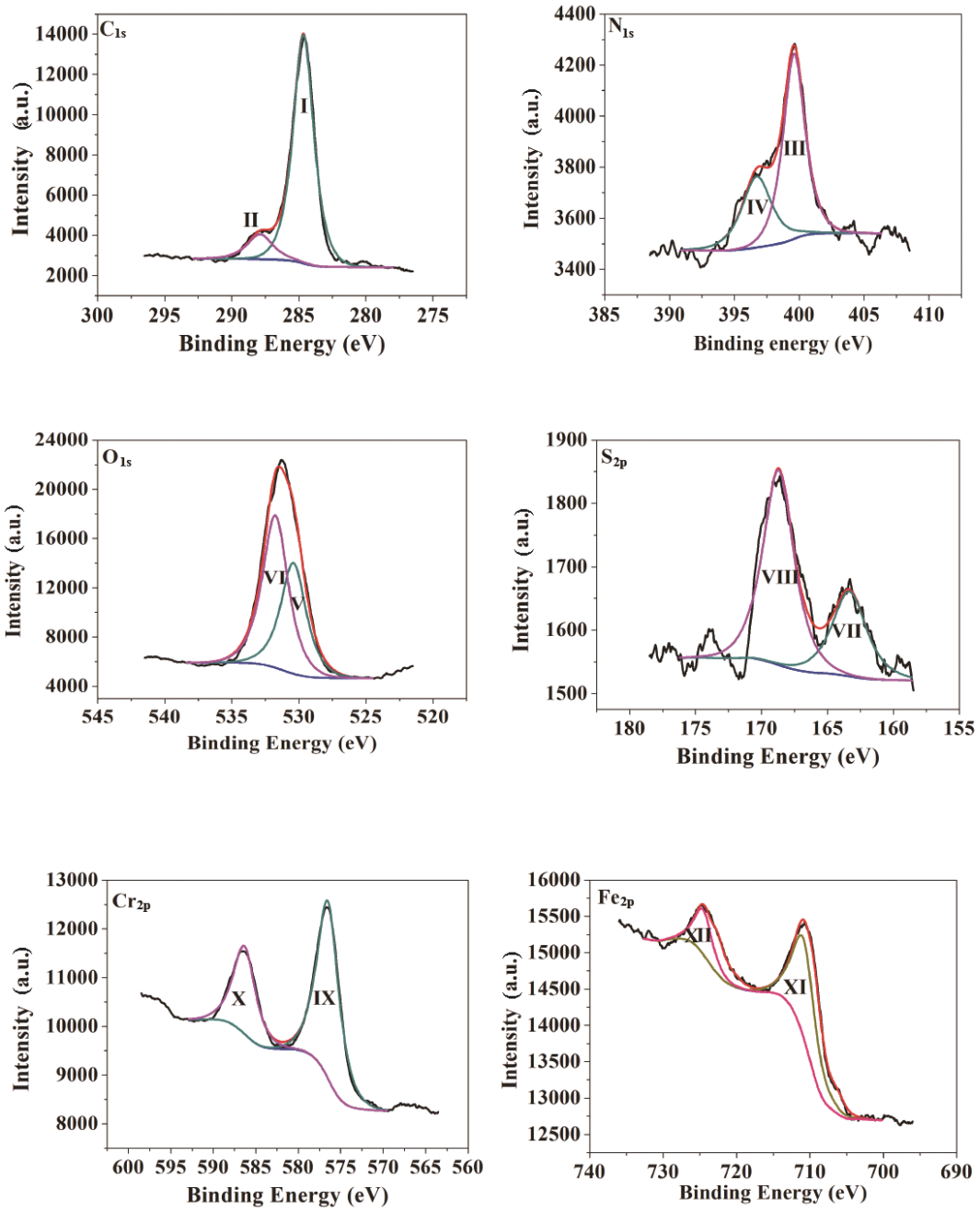

Fig.9 High resolution XPS spectra of nitrided samples after H_2S corrosion: C_{1s}, N_{1s}, O_{1s}, S_{2p}, Cr_{2p} , Fe_{2p}.

Table2 Binding energy and specification for the elements by XPS analysis of nitrided and untreated samples after H_2S corrosion

Element		BE(eV)	peak	at%
untreated				
C	1s	284.6	Adventitious/C , I	19.79
	1s	288.3	Adventitious，II	1.89
O	1s	530.7	Cr_2O_3 , III	15.46
	1s	531.7	FeOOH , IV	28.91
S	2p	162.2	FeS_2 , V	3.78
	$2p_{3/2}$	168.6	SO_4^{2-} , VI	9.40
Cr	$2p_{3/2}$	576.8	Cr_2O_3 , VII	3.90
	$2p_{1/2}$	586.8	$Cr(OH)_3$, VIII	1.66
Fe	$2p_{3/2}$	711.2	Fe_2O_3 , IX	9.65
	$2p_{1/2}$	724.3	FeOOH , X	5.56
nitrided				
C	1s	284.6	Adventitious/C, I	45.04
	1s	288.3	Adventitious，II	6.07
N	1s	396.7	CrN , III	0.98
	1s	399.6	NH_4^+, IV	1.89
O	1s	530.7	Cr_2O_3 , V	16.78
	1s	531.7	FeOOH , VI	23.16
S	$2p_{1/2}$	163.5	FeS_2 , VII	0.10
	$2p_{3/2}$	168.6	SO_4^{2-}, VIII	0.20
Cr	$2p_{3/2}$	576.5	Cr_2O_3 , IX	2.58
	$2p_{1/2}$	586.3	Cr_2O_3 , X	1.27
Fe	$2p_{3/2}$	710.8	Fe_2O_3 , XI	1.42
	$2p_{1/2}$	724.3	FeOOH , XII	0.51

Elemental contributions analyses have been performed for carbon， nitrogen， oxygen, sulfur， chromium and iron on the H_2S corrosion tested surface of untreated and as-nitrided samples and the results are reported in Figure 8 and Figure 9, respectively. The parameters and corresponding atomic contents are detailed in Table 2.

Oxygen (O_{1s}) contribution in both untreated and nitrided sample appears as two visible although entangling peaks: one for oxides at 530.7 eV and one for hydroxides at 531.7 eV.[25] XPS analysis results showed that the corrosion products formed on the untreated and nitrided samples were approximately the same, mainly Fe_2O_3, FeOOH. The corrosion products detected by XRD are mainly sulfides, whilst the corrosion products detected by XPS are mainly oxides. This is because the detection depth of the two techniques is different: the detection depth of XRD is usually in the micron range, but the XPS detection is in the nanoscale. Therefore, it can be considered that the corrosion product is layered with the oxide content enriched in the outer layer and the sulfide content in the inner layer.

The characteristic peaks of Cr in nitrided and untreated samples are mainly Cr_2O_3 and a small amount of $Cr(OH)_3$. Chromium accumulated in the corrosion product film to form a stable amorphous Cr $(OH)_3$, which makes the film more stable. At the same

time, the corrosion product film mainly containing $Cr(OH)_3$ has a certain cation selective permeability. It can effectively prevent the anion from penetrating the corrosion product film to the metal surface and reduce the corrosion rate of the material.[26] Since $Cr(OH)_3$ is amorphous,[27] it does not be detected by XRD.

For the S_{2p} fit spectrum, 162.2 eV and 163.5 eV can be considered as the peak of $FeS_{1.15}$, which is consistent with the previous analysis. 168.6 eV can be considered as a characteristic peak of sulfate, such as $FeSO_4$, $Fe_2(SO_4)_3$, etc. The presence of sulfates was not expected to be formed in H_2S electrolyte due to the absence of oxygen in solution, which could be the consequence of sulfide oxidation during the air exposition between the end of aging in the H_2S solution and the XPS measurements. For the nitrided samples, 396.7 eV can be regarded as a characteristic peak of CrN in N_{1s} fit spectrum. 399.6 eV can be regarded as a characteristic peak of NH_4^+, indicating that the active nitrogen of the nitrided layer reacts with H^+ in the H_2S solution, consumes H^+, lowers the pH and protects the metal. The experimental result is consistent with our previous finding.[28]

It can be found from Table 2 that after the H_2S corrosion, the S content (13.27 at%) and Fe content (12.51 at%) of the untreated sample are significantly larger than that of the nitrided sample (0.3 at% S and 1.93 at% Fe). On the one hand, it is shown that nitriding can prevent the formation of corrosion products on the surface of the sample, and on the other hand, it also indicates that the corrosion product is difficult to deposit on the surface of the sample. The literature indicates that under certain conditions, the corrosion product film has no protective effect on the substrate and may even lead to an increase in the corrosion rate.[29-31] Since the nitrided layer reduced the production of corrosion products, further corrosion of the sample can be prevented.

3.6 Hydrogen permeation analysis

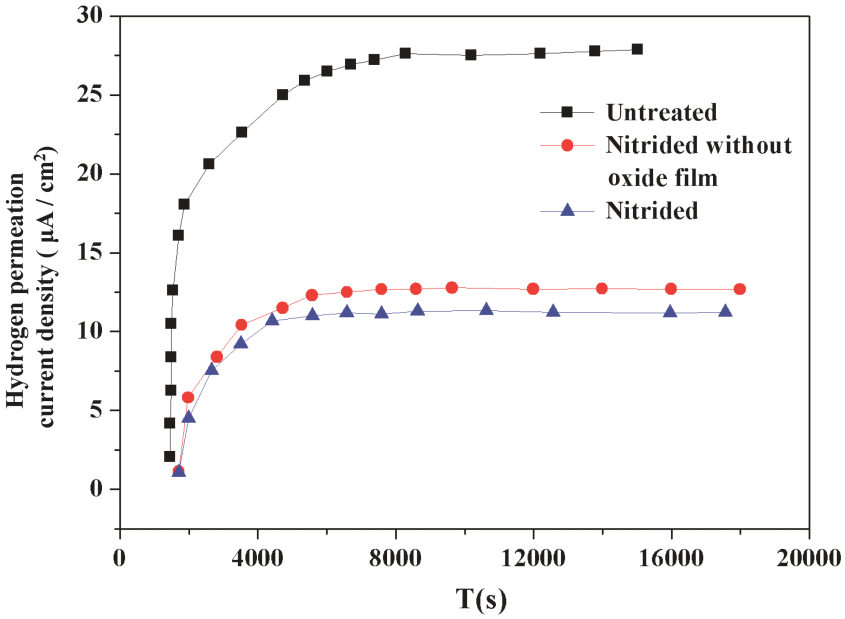

Fig.10 Hydrogen permeation current density curves of samples under different conditions.

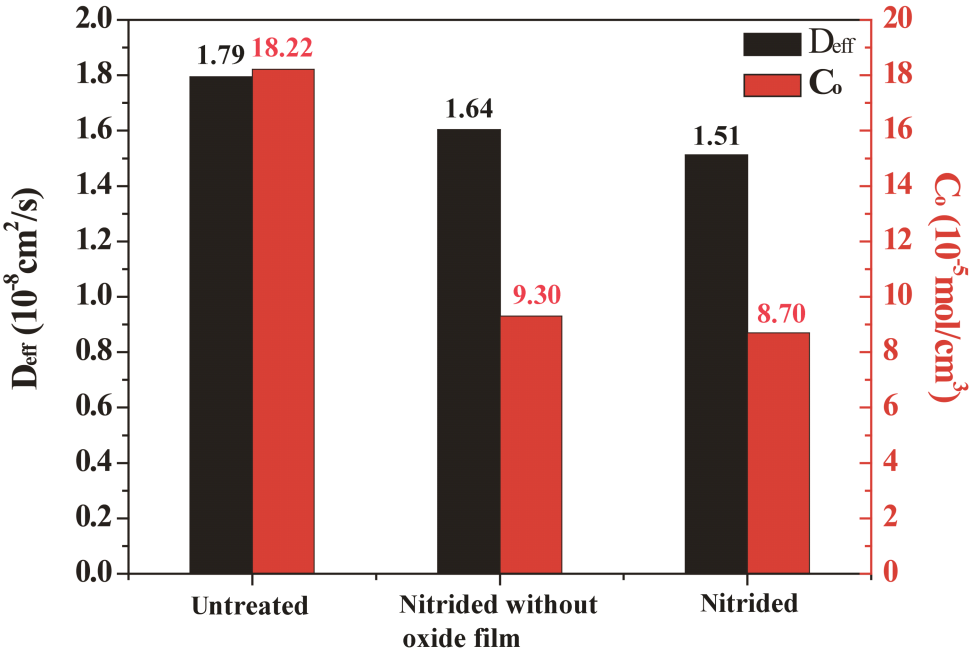

Fig .11 Diffusion coefficients and hydrogen atom concentrations curve of the sample under different conditions.

Hydrogen permeation occurring on the surface of pipe steel is one of the main risks of steel failure, and the intensity of which can be reflected in the hydrogen permeation current. [32] Zhang et al. investigated the effect of the cathodic current density (i) on the permeation of hydrogen through X80 pipeline steels using an electrochemical permeation technique and they provided an equation to describe the relationship between concentration of hydrogen (C_0) and cathodic current density (i), this equation indicated that C_0 increased with i. [33] The hydrogen permeation current density curves of different samples are shown in Figure 10. It can be seen that the anodic steady-state current density of untreated samples is significantly greater than that of as-nitrided samples and nitrided & oxide film removed samples. In addition，the untreated sample took a longer period to reach the steady state anode current density than the as-nitrided samples and the nitrided & oxide film removed samples. Figure 11 shows the hydrogen diffusion coefficient D_{eff} and hydrogen concentration C_o for different materials states. The results show that the hydrogen concentration in the untreated sample (18.22×10^{-5} mol/cm^2) is significantly higher than that of the as-nitrided sample (9.30×10^{-5} mol/cm^2) and the nitrided & oxide film removed samples (8.70×10^{-5} mol/cm^2). The reason for this may be that the nitrided layer could trap a large amount of hydrogen, thus resulting in a substantial reduction of hydrogen absorption by the substrate.[34] The hydrogen diffusion coefficient (1.79×10^{-8} cm^2/s) of the untreated sample is larger than that of the as-nitrided sample (1.64×10^{-8} cm^2/s) and nitride & oxide film removed sample (1.51×10^{-8} cm^2/s), indicating the nitrided layer and oxide layer can reduce the diffusion coefficient of hydrogen.

4. Discussion

4.1 The effect of the nitrided layer on hydrogen permeation

When the sample is soaked in the H_2S containing solution for a long time, H_2S reacts with the surface of the steel to produce hydrogen, which then enters the steel matrix，building up pressure that leads to embrittlement.[35] Research has shown that supersaturated interstitials cause large lattice expansion while the non-nitrided bulk material constrains this expansion, causing the nitrided layer to have very high residual compressive stresses.[36] Therefore, the residual compressive stress helps to relieve the tensile stress caused by the H atoms, thus preventing hydrogen embrittlement. However, when the sample is in a stress corrosion environment and the applied tensile stress increases to a certain extent, the residual compressive stress of the S-phase layer may be cancelled out and hydrogen-induced cracking can occur.[28] From the results of electrochemical hydrogen permeation experiment (Fig.10 and Fig 11), it can be seen that both the nitrided layer and the oxide layer help reduce the diffusion coefficient of hydrogen and the amount of hydrogen atoms entering the material, thus shorting the time required for the anode current to reach equilibrium. The possible reason is that the nitriding layer can trap a large amount of hydrogen, resulting in a substantial reduction of hydrogen absorption by the substrate,[34] as shown in Figure 11.

Research has shown that electrochemical H-charging of pulsed plasma nitrided austenite resulted in a softening effect within the compound layer (S-phase).[37] The hydrogen in the lattice acts as a solution softening agent and the softening or hardening effect of the hydrogen is dependent on the nitrogen concentration and the dislocation density of the material. As can be seen from Figure 7, the nitrogen concentration exceeds 20 at%. When hydrogen ions enter the nitrided layer with a very high interstitial atom content, it softens and prevents hydrogen embrittlement.

4.2 The effect of the nitriding on H_2S corrosion

Figure 12 schematically shows the H_2S corrosion model for untreated and nitrided specimens. As shown in Figure 12(a), acidic H_2S solution hydrolyzes H^+, HS^-, S^{2-}，which reacts on the surface of the steel to produce Fe^{2+}. When acidic chemical corrosion occurs, the inherent protective film on the pipe surface is destroyed, causing the corrosive medium to enter the interior of the metal crystal and generating electrochemical corrosion. Electrochemical corrosion forms an etched primary cell. The anode process is a dissolution reaction of the metal, and the cathode undergoes a hydrogen depolarization reaction. Anodic sulphide corrosion products deposit on the metal surface, which is poorly protective and in fact promotes the corrosion of the stainless steel substrate. Monnot et al. highlighted the role of corrosion products on the failure mechanism of martensitic stainless steels in sour media.[38] Corrosion product formed under this condition has a high level of porosity and is prone to spalling due to cracks and defects throughout the amorphous structure. In fact, H_2S diffuses on the surface of the etching film and penetrates along the porous structure, and reacts at the metal/film interface. The metal sulphide is formed to release the hydrogen previously bound to the sulfur that can be absorbed by the alloy. Corrosion

product films therefore correspond to a rich hydrogen reservoir near the metal surface that can trigger and maintain hydrogen uptake. The data in Table 2 show that nitriding treatment can effectively reduce the generation of corrosion products, thereby alleviating hydrogen embrittlement and corrosion.

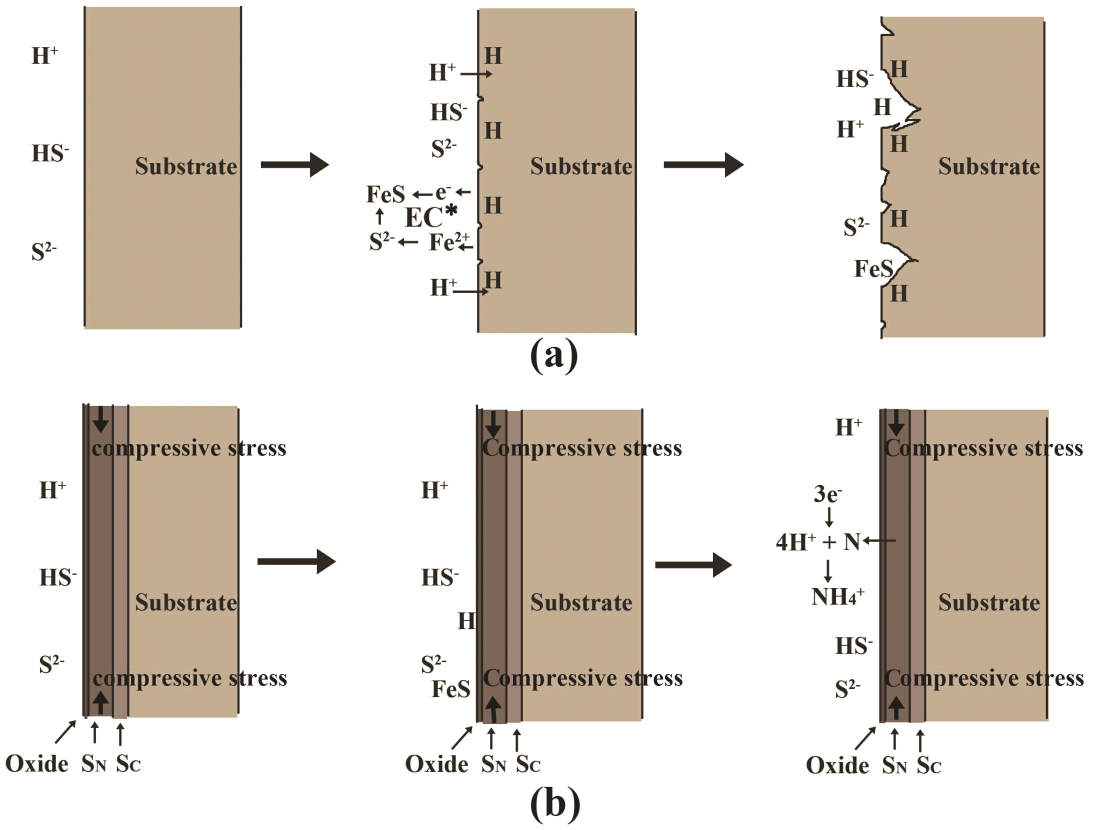

Note:* stands for electrochemical corrosion.

Fig.12 H_2S corrosion model of (a) untreated sample and (b) nitrided sample

The oxide layer can effectively prevent the corrosion of acidic H_2S as schematically shown in Figure 12(b). Granda—Gutiérrez et al. found that post-oxidation following nitriding treatment increased the time to SSC rupture of stainless steel by a factor of 10 because the dense oxide film on the surface after the treatment significantly improved the resistance to H_2S corrosion cracking of the stainless steel.[39] This is partially because the nitride layer reduced the generation of corrosion products (Table 2) and partially because it also prevented hydrogen atoms (Fig.11) from entering the substrate, thereby preventing electrochemical corrosion.

Nitrogen can effectively improve the local corrosion resistance of stainless steel,[40] and some hypotheses have been put forward to explain this behavior: (1) high concentration of nitrogen atoms on the surface of stainless steel stabilizes passive film and inhibits dissolution;[41-43] (2)formation of NO_3^- (nitrate) ions leads to increased pitting resistance;[44] (3) stabilization effect of nitrogen on austenite.[45] For the nitrided samples produced in this research, there are a large amount of active nitrogen

atoms in the surface of the sample after low temperature nitriding due to the high level of chromium, nickel, molybdenum in the matrix material . The fitted spectra of N1s from the nitriding samples after being soaked in H_2S solution are shown in Figure 9. H^+ reacts with the nitrogen atom via the reaction： $N + 4H^+ = NH_4^+$. This consumed the H^+ in the solution prevented the pH of the metal surface from decreasing, and thereby increased the corrosion resistance of the alloy, which is consistent with the EPMA results in Figure7. At the same time, the active nitrogen atoms can accelerate the formation of passivation film and affect the repassivation kinetics, so that the passivation film can grow stably and increase the density of the passivation film.[46]

5. Conclusions

Low-temperature liquid nitrided samples have better corrosion resistance than untreated samples in H_2S environment. The corrosion rate of the untreated sample is about 3.6 times that of the nitriding sample; clear corrosion pits can be observed on the surface of the untreated sample, while the treated sample surface remains almost intact. Due to the presence of oxide layers, despite precipitation of CrN in the nitriding layer, the corrosion resistance of the sample after the nitriding treatment in the H_2S environment is still significantly improved by the treatment.

The corrosion products are mainly consisted of oxides, hydroxides, and sulfates. The nitrided layer reduces the production of corrosion products; further corrosion of the sample is thus prevented. Both oxide layer and nitrided layer can reduce the diffusion coefficient of hydrogen and the amount of hydrogen atoms entering the material, which is beneficial to improving the resistance to hydrogen embrittlement. Nitriding layer is supersaturated with active nitrogen atoms, which combine with H^+ to avoid surface pH reduction, thus decelerating H_2S corrosion.

Acknowledgement

The authors are very grateful to the grants provided by National Natural Science Foundation of China (No. 51471112 and 51611130204), Science and Technology Planning Project of Sichuan (No.2016GZ0173) and the Newton Mobility Grant from Royal Society, UK (IE151027).

References

1. K. Komai, *Int. J. Fatigue.,* 1998, vol. 20, pp. 145-154.
2. M. L. Medvedeva and V. V. Gur'Yanov, *Prot. Met.,* 2002, vol. 38, pp. 284-288.
3. D. W. Shoesmith, P. Taylor, M. G. Bailey and D. G. Owen, *Cheminform,* 1980, vol. 11, pp. 1007-1015.
4. H. Yang, J. Chen, C. Cao, D. Cao and X. Jiang, *J .Chin. Soc. Corros . Rrot.,* 2001, vol. 21, pp. 321-327.
5. H. Wang, P. Zhou, S. Huang, C. Yu, *Int. J. Electrochem. Sci.,* 2016, vol. 11, pp. 1293-1309.
6. J. Fliethmann, H. Schlerkmann and W. Schwenk, *Corros. Sci.,*1992, vol. 24, p. 746.
7. J. Ding, Z. Lei, M. Lu, J. Xue and Z. Wen, *J. Mater. Sci. Technol.,* 2013, vol. 48, pp. 3708-3715.
8. S. K. Putatunda, *Mat. Sci. Eng. R.,* 1986, vol. 82, pp. L7-L11.

9. W.T. Tsai and S.L. Chou, *Corros. Sci.,* 2000, vol. 42, pp. 1741-1762.
10. L. F. Li, Z. Q. Huang and X. M. Liu, *Adv. Mater.,* 2012, vol. 485, pp. 393-396.
11. A. Heuer and S. Collins, *Metall. Mater. Trans. A.,* 2009, vol. 40, pp. 1767-1767.
12. G. M. Michal, F. Ernst, H. Kahn, Y. Cao, F. Oba, N. Agarwal and A. H. Heuer, *Acta. Mater.,* 2006, vol. 54, pp. 1597-1606.
13. X. Y. Li and H. Dong, *Met. Sci. J.,* 2003, vol. 19, pp. 1427-1434.
14. S.J.B.Kurza, S.R.Mekaa, N.Schellb, W.Eckerc, J.Keckesd, E.J.Mittemeijerae, *Acta. Mater.*, 2015, vol. 87,pp.100-110.
15. L. Zhang, C. Ren, Q. Yu, J. Zhang, S. Sun, Q. Ren, Y. Lian, X. Chen and W. Gao, *Surf. Coat. Technol.,* 2017, vol. 315, pp. 95-104.
16. J. Wang, Y. Lin, J. Yan, D. Zeng, R. Huang and Z. Hu, *Isij Int.,*2012, vol. 52, pp. 1118-1123.
17. M. A. V. Devanathan, Z. Stachurski, *Proc. Royal. Soc. Lond,* 1962, vol. 270(1340), pp. 90-102
18. S. Shen, X. Li, P. Zhang, Y. Nan, G. Yang: *Mater. Sci. Eng. A* 2017, vol. 703, pp: 413-421
19. H. Hu, K. Li, W. Wu, G.X.Chen, W.J.Chen: *J. Xi'an Jiaotong Univ*. 2016, vol. 50(07). 89-95.
20. C. Zhou, S. Zheng, C. Chen and G. Lu, *Corros. Sci.,* 2013, vol. 67, pp. 184-192.
21. R.A. Carneiro, R. C. Ratnapuli and V. D. F. C. Lins, *Mat. Sci. Eng. A.,* 2003, vol. 357, pp. 104-110.
22. C. F. Dong, Z. Y. Liu, X. G. Li and Y. F. Cheng, *Int. J. Hydrogen. Energ.,* 2009, vol. 34, pp. 9879-9884.
23. M. Tsujikawa, N. Yamauchi, N. Ueda, T. Sone and Y. Hirose, *Surf. Coat. Technol.,* 2005, vol. 193, pp. 309-313.
24. W. Shi, X. Y. Li and H. Dong, *Wear.,* 2001, vol. 250, pp. 544-552.
25. M. Mantel and J. P. Wightman, *Surf. Interface. Anal.,* 1994, vol. 21, pp. 595-605.
26. C. F. Chen, W. F. Chang, Z. H. Zhang, M. X. Lu and D. B. Sun, *Corrosion -Houston Tx-* 2005, vol. 61, pp. 594-601.
27. J. Sun, C. Sun, X. Lin, X. Cheng and H. Liu, *Materials.,* 2016, vol. 9, p. 200.
28. X. Zhang, J. Wang, H. Fan, J. Yan, L. Duan, T. Gu, G. Xian, L. Sun and D. Wang, *Metall. Mater. Trans. A.,*2018, vol. 49, pp. 356-367.
29. D. R Morris, L. P Sampaleanu and D. N Veysey, *J. Electrochem. Soc.,* 1980, vol. 127, pp. 1228-1235.
30. F. H. Meyer, O. L. Riggs, R. L. Mcglasson and J. D. Sudbury, *Corrosion -Houston Tx-* 1958, vol. 14, pp. 109-115.
31. J. S. Smith and J. D. A. Miller, *Brit. Corros. J.,* 2013, vol. 10, pp. 136-143.
32. C. Zhou, X. Chen, Z. Wang, S. Zheng, X. Li, L. Zhang, Corros. Sci. 2014, vol. 89, pp: 30-37
33. L. Zhang, W. Cao, K. Lu, Z. Wang, Y. Xing, Int. J. Hydrogen Ener, 2017, vol. 42(5), pp: 3389-3398.
34. T. Zakroczymski, J. Flis, N. Lukomski and J. Mankowski, *Acta.Mater.,* 2001, vol. 49, pp. 1929-1938.
35. Z. Y. Liu, C. F. Dong, X. G. Li, Q. Zhi and Y. F. Cheng, *J. Mater. Sci.,* 2009, vol. 44, pp. 4228-4234.
36. A. H. Heuer, F. Ernst, H. Kahn, A. Avishai, G. M. Michal, D. J. Pitchure and R. E. Ricker, *Scripta Mater.,* 2007, vol. 56, pp. 1067-1070.
37. M. Asgari, A. Barnoush, R. Johnsen and R. Hoel, *Corros. Sci.,* 2012, vol. 62, pp. 51-60.
38. M. Monnot, R.P. Nogueira, V. Roche, G. Berthomé, E. Chauveau, R. Estevez,M. Mantel, *Appl.*

524 *Surf. Sci.*, 2017, 394:132-141.
525 39. E. E. Granda-Gutiérrez, J. C. Díaz-Guillén, J. A. Díaz-Guillén, M. A. González, F.
526 García-Vázquez and R. Muñóz, *J. Mater. Eng. Perform.,* 2014, vol. 23, pp. 4148-4153.
527 40. P. G. Esteban, L. Bolzoni, E. M. Ruiznavas and E. Gordo, *Power. Metall.,* 2011, vol. volume 54,
528 pp. 242-252(11).
529 41. Y. C. Lu, R. Bandy, C. R. Clayton and R. C. Newman, *Cheminform.,* 1983, vol. 14, pp.
530 1774-1776.
531 42. H. Baba, T. Kodama and Y. Katada, *Corros. Sci.,* 2002, vol. 44, pp. 2393-2407.
532 43. C.O. A. Olsson, *Corros. Sci.,* 1995, vol. 37, pp. 467-479.
533 44. H. P. Leckie, *J.electrochem. soc.,* 1966, vol. 113, pp. 1262-1267.
534 45. J. W. Simmons, *Mat. Sci. Eng. A.,* 1996, vol. 207, pp. 159-169.
535 46. P. R. Levey and A. R. V.Bennekom, *Corrosion.,* 1995, vol. 51, pp. 911-921.

Fig.1 A typical cross sectional SEM image of nitrided sample

Fig.2 Cross-sectional optical micrographs (OM): (a) untreated sample (b) nitrided sample after immersion in H_2S solution for 720h

Fig.3 SEM surface corrosion morphology: (a) untreated sample (b) nitrided sample after immersion in H_2S solution for 720h

Fig.4 Corrosion rate after H_2S corrosion for 720h

Fig.5 XRD patterns for different samples: (a) nitrided sample after corrosion test, (b) untreated sample after corrosion test, (c) as-nitrided sample and (d) untreated sample before corrosion test

Fig. 6 XRD patterns as a function of the depth below the original nitrided surface (after mechanical material removal).

Fig.7 EPMA results of untreated (a) and nitrided samples (b) after immersion corrosion test in Solution A for 720h

Fig.8 High resolution XPS spectra of untreated samples after H_2S corrosion: C1s, O1s, S2p, Cr2p, Fe2p.

Fig.9 High resolution XPS spectra of nitrided samples after H_2S corrosion: C1s, N1s, O1s, S2p , Cr2p , Fe2p .

Fig.10 Hydrogen permeation current density curves of samples under different conditions.

Fig.11 Diffusion coefficients and hydrogen atom concentrations curve of the sample under different conditions.

Fig.12 H_2S corrosion model of (a) untreated sample and (b) nitrided sample

Table 1 Chemical composition of AISI 304 stainless steel (mass%)

Table 2 Binding energy and specification for the elements by XPS analysis of nitrided and untreated samples after H_2S corrosion